# Ni-Based Catalysts for the Hydrotreatment of Fast Pyrolysis Oil

Ardiyanti, A. R.; Bykova, M. V.; Khromova, S. A.; Yin, W.; Venderbosch, R. H.; Yakovlev, V. A.; Heeres, Hero

*Published in:*
Energy & fuels

*DOI:*
10.1021/acs.energyfuels.5b02223



*Publication date:*
2016

energy&fuels

Article

pubs.acs.org/EF

# Ni-Based Catalysts for the Hydrotreatment of Fast Pyrolysis Oil

A. R. Ardiyanti,[†] M. V. Bykova,[‡,§] S. A. Khromova,[‡] W. Yin,[†] R. H. Venderbosch,[∥] V. A. Yakovlev,[‡] and H. J. Heeres*[,†]

[†]Department of Chemical Engineering, University of Groningen, Nijenborgh 4, 9747 AG Groningen, Netherlands

[‡]Boreskov Institute of Catalysis, 5 Akademika Lavrentieva Prospect, 630090 Novosibirsk, Russia

[§]Novosibirsk State University, 2 Pirogova Street, 630090 Novosibirsk, Russia

[∥]Biomass Technology Group BV, Josink Esweg 34, 7545 PN Enschede, Netherlands



**ABSTRACT:** Catalytic hydrotreatment is an attractive technology to convert fast pyrolysis oil to stabilized oil products for co-processing in conventional crude oil refinery units. We report here the use of novel bimetallic NiCu- and NiPd-based (Picula) catalysts characterized by a high Ni content (29−58 wt %) and prepared using a sol−gel method with $SiO_2$, $La_2O_3$, kaolin, $ZrO_2$, and combinations thereof as the support, for the catalytic hydrotreatment of fast pyrolysis oil. The experiments were performed in a batch autoclave (1 h at 150 °C, 3 h at 350 °C, and 200 bar initial pressure at 350 °C). The catalyst with the highest nickel loading (58 wt % Ni) promoted with Pd (0.7 wt %) was the most active, yielding oil products with improved properties compared to the crude pyrolysis oil (lower oxygen content, higher solubility in hydrocarbons, and less tendency for coke formation). For all Picula catalysts, except the $ZrO_2$-based catalysts, methane formation was considerably lower than for Ru/C, the benchmark catalyst in catalytic hydrotreatment of fast pyrolysis oil. To anticipate possible catalyst deactivation at very long times on stream, catalyst regeneration studies were performed using thermogravimetric analysis. Analyses of the regenerated catalysts (X-ray diffraction, high-resolution transmission electron microscopy, and Brunauer−Emmett−Teller surface area) showed the occurrence of active metal agglomeration.

## 1. INTRODUCTION

Lignocellulosic biomass is abundantly available and an attractive renewable feed for the production of second-generation biofuels.[1] Various liquefaction technologies have been proposed to improve the volumetric energy density ($MJ/m^3$) of biomass to simplify and reduce the cost for transportation. A close to commercial technology is fast pyrolysis.[2−5] During fast pyrolysis, the biomass feed is heated rapidly in the absence of oxygen to 400−600 °C. The main product is fast pyrolysis oil (PO, also referred to as "pyrolysis oil" or "bio-oil"), obtained in yields up to 70 wt % on a dry biomass basis. It is a viscous, brown oil that contains considerable amounts of water (between 20 and 35 wt %). It is immiscible with petroleum products and acidic and has limited storage stability because of the occurrence of irreversible oligo- and polymerization reactions.[6] As a result of these unfavorable characteristics, its application potential is still rather limited, for instance as a fuel in boilers (with modified injection systems) and as a co-feed in existing power plants.

It is evident that fast pyrolysis oils require upgrading/modification for various applications to improve product properties, to be more specific (i) to reduce the acid content (to avoid excessive corrosion), (ii) to improve thermal stability (and, in particular, the tendency for coke formation upon storage and heating), and (iii) preferably to enhance the miscibility with petroleum feeds.

Upgrading of pyrolysis oil for use as a co-feed in existing oil refineries has been explored,[7−10] with the incentive to substitute part of the gasoline and diesel by renewable carbon without the need to develop new infrastructure for distribution and handling. Examples of upgrading technologies are catalytic and non-catalytic thermal treatments.[8,11−20] In particular, a catalytic treatment using hydrogen appeared very interesting. Catalytic hydrotreatment of pyrolysis oil is a process where the oil is reacted with hydrogen in combination with a solid catalyst. Co-processing of such hydrotreated pyrolysis oils (20 wt %, obtained over Ru/C) together with long residue fractions was performed in a lab-scale simulated fluidized catalytic cracking (FCC) unit (MAT),[8] resulting in yields close to those obtained for 100% long residue. Interestingly, no excessive increase of undesired coke and dry gas was observed.

Catalytic hydrotreatment, sometimes referred to as hydrodeoxygenation (HDO), actually involves a combination of reactions, such as polymerization, (hydro)cracking, deoxygenation, and hydrogenation. Elevated temperatures (250−450 °C) and pressures (140−200 bar) are required,[14,21] and typical catalysts include supported noble metal systems (Rh, Pd, Pt, and Ru)[22] and Ni-based metal catalysts.[23,24] On the basis of process studies using Ru/C catalysts, a reaction network for the catalytic hydrotreatment of fast pyrolysis oil has been proposed by Venderbosch et al.[21] (see Scheme 1).

In the initial phase of the hydrotreatment process, catalytic hydrogenation and thermal, non-catalytic polymerization occur in a parallel mode. Polymerization, mainly of reactive (small) aldehydes, such as hydroxyacetaldehyde and carbohydrates (e.g., $C_6$ sugars, such as glucose), leads to the formation of soluble

**Special Issue:** 5th Sino-Australian Symposium on Advanced Coal and Biomass Utilisation Technologies

**Received:** September 26, 2015
**Revised:** December 27, 2015
**Published:** December 28, 2015

  

DOI: 10.1021/acs.energyfuels.5b02223
*Energy Fuels* 2016, 30, 1544−1554

**Scheme 1. Proposed Reaction Pathway for the Catalytic Hydrotreatment of Pyrolysis Oil[21]**

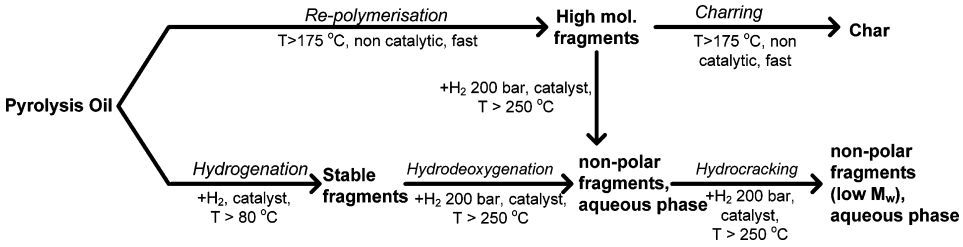


higher molecular weight fragments, which upon further condensation reactions give char. This route is not preferred, and the rate of the polymerization reactions should be reduced as much as possible. The preferred pathway involves hydrogenation of the thermally labile components in the pyrolysis oil feed to stable molecules that are not prone to polymerization. Subsequent reactions (hydrodeoxygenation and hydrocracking) on a time scale of hours lead to products with reduced oxygen contents and ultimately to higher H/C ratios.

Catalyst development in hydrotreating of fast pyrolysis oils is key, because most catalysts are (i) not sufficiently active at temperatures below 200 °C to avoid thermal repolymerization and (ii) not stable and decay within (tenths of) hours. We recently reported the use of cheaper Ni-based catalysts as active and selective alternatives to noble-metal-based catalysts. Bimetallic NiCu catalysts on various supports ($\delta$-$Al_2O_3$, $CeO_2$–$ZrO_2$, $ZrO_2$, $SiO_2$, $TiO_2$, rice husk carbon, and sibunite) with an active metal loading with a maximum of 25 wt % were prepared by wet impregnation, tested, and indeed led to products with improved properties.[25,26] However, the rate of hydrogenation in the initial stage of the reactions appears still relatively low, and conditions are such that also thermal polymerization reactions occur to some extent. The development of more active hydrogenation catalysts is thus highly desirable.

In this study, we report the use of a new family of hydrotreating catalysts based on bimetallic NiCu and NiPd complexes, referred to as Picula catalysts. These catalysts are prepared by a sol–gel method and characterized by a high metal loading (>32 wt %, typically >50 wt %). The sol–gel method was selected because it is known to allow for the synthesis of a supported metal catalyst with a high metal loading in combination with small metal nanoparticle sizes, a prerequisite for high catalytic activity.[27]

Silica was the support of choice because it is known to form silicate-like structures, which stabilize small Ni particles in the silica matrix after the reduction.[27] $ZrO_2$ was added to the catalyst composition with the objective to obtain catalysts with improved mechanical strength and thermal stability. In addition, in one of the formulations, $La_2O_3$ was added as a promotor to further improve the thermal stability of $ZrO_2$.[28] A catalyst with a high Ni content (Raney nickel) has been reported as a catalyst for hydrodeoxygenation of a pyrolysis oil model compound (4-*n*-propylphenol),[29,30] but to the best of our knowledge, the use of such catalysts has not been reported for the catalytic hydrotreatment of fast pyrolysis oils and is a novelty of this paper.

Catalyst-screening studies were performed in a batch setup to gain insights in the catalytic activity of the various catalysts. Relevant product properties of the oil products were determined. Spent catalysts were characterized and regenerated to gain insights in catalyst deactivation pathways and potential reuse of the catalysts.

## 2. MATERIALS AND METHODS

**2.1. Materials.** Fast pyrolysis oil used in this study was produced by VTT (Espoo, Finland) and obtained by fast pyrolysis of pine wood. The elemental composition of the oil is given in Table 1. Ru/C (5 wt % Ru, a surface area of 717 $m^2/g$, and a surface-weighted mean diameter of 6.8 $\mu$m) was obtained from Sigma-Aldrich. Hydrogen (purity of >99.999%) was purchased from Linde.

**Table 1. Composition of the PO Used in This Study[a]**

| | amount (wt %) |
|---|---|
| C (wb) | 40.1 |
| H (wb) | 7.6 |
| N (wb) | 0.1 |
| S (wb) | 0.01 |
| O (by difference, wb) | 52.1 |
| O (db) | 40.1 |
| water content | 23.9 |
| atomic O/C (db) | 0.56 |
| atomic H/C (db) | 1.47 |

[a]wb, wet basis; db, dry basis.

**2.2. Catalyst Preparation, Regeneration, and Characterization.** *2.2.1. Catalyst Preparation.* NiCu/$SiO_2$ (cat D) was prepared by a sol–gel method, and details are provided elsewhere.[27,31] The appropriate amounts of commercial precursors were dissolved in water and mixed with 25% $NH_3$ solution. Subsequently, a solution of ethyl silicate was added to yield the catalyst after drying and calcination. NiPd/$SiO_2$ (cat B) was prepared by the same method as given above for cat D but using Pd instead of Cu. NiCu/$SiO_2$–kaolin (cat C) was prepared by mechanical mixing of cat D with kaolin. NiCu/$SiO_2$–$ZrO_2$–$La_2O_3$ (cat E) was prepared using a similar procedure as for cat D, except that $ZrO_2$ and $La_2O_3$ precursors were added after the addition of ethyl silicate.

*2.2.2. Catalyst Regeneration Studies.* Catalyst regeneration protocols are based on the results of thermogravimetric analysis (TGA) (*vide infra*). Regeneration was performed under static air. For the determination of the optimum calcination temperature for the spent catalysts, two calcination modes were applied. The isothermal mode involved heating the catalysts to a preset temperature of 300 °C and keeping the sample at this temperature for 1 h. Calcination in the dynamic mode involved heating the catalysts with a constant heating rate of 10 °C/min from ambient temperature to 600 °C.

The following procedure was applied for the regeneration of the catalysts to be further characterized by a number of physicochemical methods [X-ray diffraction (XRD), high-resolution transmission electron microscopy (HRTEM), and $N_2$ physical adsorption]. The samples were heated from ambient temperature to 300 °C at a constant heating rate of 10 °C/min and kept for 1 h at this temperature. Next, the temperature was increased to 400 °C. Once this temperature was reached, heating was ceased and the samples were allowed to cool to room temperature. The final calcination temperature did not exceed 400 °C, because fresh catalysts were also calcined at this temperature. Thus, treated samples were further reduced for 1 h at 350 °C and 0.1 MPa $H_2$ (flow rate of 100 $cm^3$/min) and characterized.



DOI: 10.1021/acs.energyfuels.5b02223
*Energy Fuels* 2016, 30, 1544–1554

*2.2.3. Catalyst Characterization. 2.2.3.1. Temperature-Programmed Reduction (TPR).* TPR studies of the catalysts were performed in a reductive medium consisting of 10% $H_2$ with 90% Ar at a flow rate of 30 mL/min and 0.1 MPa. The catalyst intake was based on constant metal intake ($m_{metal}$ = 50 mg), and as such, the total sample intake (metal + support) was variable. Catalyst samples were placed in a quartz reactor (U-tube) and were heated with a constant heating rate of 6 °C/min until 800 °C. The hydrogen concentration in the outlet stream during reduction was measured by a thermal conductivity detector (TCD).

*2.2.3.2. $N_2$ Physical Adsorption.* Texture characteristics of the catalysts were measured at the liquid nitrogen temperature using an ASAP-2400 automated volumetric adsorption analyzer (Micromeritics Instrument Corp., Norcross, GA). Before the analysis, the samples were degassed at 150 °C and a pressure of 0.13 Pa for 4 h. The analysis time was varied depending upon the particular sample. The resulting adsorption isotherms were used to calculate the specific surface area $A_{BET}$, the total pore volume $V_{\Sigma}$ (from ultimate adsorption at a relative pressure of $P/P_0 = 1$), the micropore volume $V_{\mu pore}$, and the mean pore size $\langle d \rangle$.

*2.2.3.3. XRD.* XRD analyses were performed on a D500 Siemens (Germany) using monochromatic Cu K$\alpha$ radiation ($\lambda$ = 1.5418 Å). Diffraction patterns were recorded by scanning with 0.05° increments at an angle range $2\theta$ from 15° to 70° using an accumulation period of 3 s per measurement. The mean coherent scattering domain (CSD) sizes of the metal crystallites were derived from the half widths of the reflections using the Selyakov−Scherrer equation.[32]

*2.2.3.4. HRTEM.* HRTEM images of selected samples were obtained from a JEM 2010 electron microscope (JEOL, Japan) at an accelerating voltage of 200 kV and a resolution of 0.14 nm. Catalyst samples were deposited onto a copper grid by dispersing an ethanolic catalyst suspension using an ultrasonic disperser.

*2.2.3.5. TGA.* TGAs of spent catalysts were performed on a thermogravimetric analyzer SHIMADZU-DTG-60H (Japan). Catalyst samples (0.01 g) placed in corundum crucibles were heated with a constant heating rate of 10 °C/min from ambient temperature to (i) 300 °C while maintaining this temperature for 1 h (isothermal mode) and to (ii) 600 °C (dynamic mode). All measurements were carried out under air (0.1 MPa).

**2.3. Hydrotreatment of Fast Pyrolysis Oil in a Batch Setup.** The hydrotreatment reactions using fast pyrolysis oil were performed in a 100 mL Parr reactor equipped with an overhead stirrer. Details of the setup are given in previous papers.[16,23,24,33] The reactor was filled with 1.25 g of catalyst and pre-reduced using 10 bar of $H_2$ at 350 °C for 1 h. After reduction, the reactor was cooled to room temperature and 25 g of fast pyrolysis oil was injected. The reactor was then flushed with $H_2$ and, subsequently, pressurized with $H_2$ to 120 bar. The reactor was operated for 1 h at 150 °C while being stirred at 1300 rpm, and subsequently, the temperature was increased to 350 °C. The reactor was operated at 350 °C for another 3 h, after which the reactor was cooled to room temperature. A sample from the gas phase was taken at room temperature and analyzed with gas chromatography−thermal conductivity detector (GC−TCD). After opening the reactor, the liquid and solid phases were collected and centrifuged to separate the aqueous phase, organic phase (oil product), and solids (including the spent catalyst). The weight of all phases was used as input for mass balance calculations. The organic phase was analyzed using various techniques (see section 2.4). The solid phase after liquid separation was washed with acetone and dried. The amount of char on the catalyst was calculated from the weight difference of the spent (acetone rinsed and dried) catalyst and fresh catalyst intake.

**2.4. Analyses of the Reaction Products.** *2.4.1. GC−TCD.* The composition of the gas phase from each experiment was determined using GC−TCD. HP5890 Series II GC equipped with CP Porabond Q (50 m × 0.5 mm, with a film thickness of 10 $\mu$m) and CP-Molsieve 5A (25 m × 0.53 mm, with a film thickness of 50 $\mu$m) columns was used for this purpose. The injector temperature was set at 150 °C, and the detector temperature was set at 90 °C. The oven temperature was kept at 40 °C for 2 min, then increased to 90 °C at 20 °C/min, and kept at this temperature for 2 min. Helium was used as the carrier gas.

*2.4.2. Elemental Analysis (EA).* The elemental composition of the oil products and the water phases after reaction was determined using an EuroVector EA3400 Series CHNS-O with acetanilide as the reference. The amount of oxygen was determined by difference.

*2.4.3. Water Content.* The water content of the liquid organic phases was determined by volumetric Karl Fischer using a Metrohm 702 SM Titrino. About 0.01 g of sample was introduced to an isolated glass chamber containing hydranal solvent (Riedel de Haen). The titration was carried out using hydranal titrant 5 (Riedel de Haen).

*2.4.4. TGA.* TGA data of the liquid organic phases were determined using TGA 7 from PerkinElmer. The samples were heated in a nitrogen atmosphere with a heating rate of 10 °C/min and a temperature range between 20 and 900 °C.

*2.4.5. Gel Permeation Chromatography (GPC).* GPC analyses of the liquid organic phases were performed using an Agilent HPLC 1100 system equipped with a refractive index detector. Three columns in series of mixed type E (length of 300 mm and inner diameter of 7.5 mm) were used. Polystyrene was used as a calibration standard. The organic phases were dissolved in tetrahydrofuran (THF, 10 mg/mL) and filtered (pore size of 0.2 $\mu$m) before injection.

*2.4.6. Proton Nuclear Magnetic Resonance ($^1$H NMR).* $^1$H NMR spectra of the crude fast pyrolysis oil and the organic product phases were recorded on a Varian AS400 at 400 MHz. The samples were dissolved in $CDCl_3$, dried over $MgSO_4$ to remove water, and filtered. For $^1$H NMR spectra, 64 repetitions and a 1 s relaxation delay were applied.

*2.4.7. Gas Chromatography−Mass Spectrometry/Flame Ionization Detector (GC−MS/FID).* GC−MS/FID measurements of the fast pyrolysis oil and the organic phase of the hydrotreatment (oil product) were performed at the Johann Heinrich von Thünen Institute (vTI, Hamburg, Germany). All GC analyses were carried out on an Agilent 6890 systems coupled with parallel FID and MS detector. Electron impact mass spectra were obtained using a 70 eV ionization energy. The GC split was 1:15; the injector temperature was 250 °C; and an injection volume of 1 $\mu$L was applied. The temperature program for the oven was as follows: 45 °C for 4 min, heating with 3 °C/min to 280 °C, followed by 20 min at 280 °C. Helium was used as the carrier gas with a constant flow rate of 2 mL/min.

*2.4.8. Solubility Tests.* The solubility of the oil products in a hydrocarbon mixture was determined by mixing 1 g of oil product with 2 g of an equimass mixture of *n*-hexane and benzene in a 10 mL test tube. The mixture was stirred in an ultrasonic bath for 5 min, heated to 40 °C for 30 min, and allowed to phase separate overnight at room temperature. The top phase, which was rich in *n*-hexane and benzene, was separated and weighed.

**2.5. Definitions.** *2.5.1. Batch Experiments.* The $H_2$ uptake for each experiment was calculated on the basis of pressure and temperature recordings and gas-phase compositions before and after the reaction and is expressed as $NL/kg_{PO}$. Details of the calculations are already given by Ardiyanti.[34] The activity of the catalyst is determined from the $H_2$ uptake, catalyst intake, and batch time (eq 1) and expressed as $NL_{H_2}\ kg_{PO}^{-1}\ g_{cat}^{-1}\ h^{-1}$. Here, the activity may be based on either the total catalyst intake or the amount of active metals (sum of Ni and Cu/Pd) in the catalyst formulation.

$$\text{catalyst activity} = \frac{H_2\ \text{uptake}}{m_{\text{catalyst}} \times \text{time}} \tag{1}$$

*2.5.2. Product Properties.* The solubility of the oil products in the hexane−benzene mixture was estimated as

$$\text{solubility} = \frac{m_{\text{HB-rich layer}} - m_{\text{HB initial}}}{m_{\text{HB initial}}} \times 100\% \tag{2}$$

where $m_{\text{HB-rich layer}}$ is the mass of the hexane−benzene-rich layer after equilibration and phase separation and $m_{\text{HB initial}}$ is the intake of the hexane−benzene mixture.

The TG residue is defined as the residue after heating a liquid product sample under a nitrogen atmosphere to 900 °C in a thermogravimetric analyzer. This parameter is an indicator for the thermal stability of the oil product.



DOI: 10.1021/acs.energyfuels.5b02223
*Energy Fuels* 2016, 30, 1544−1554

**Table 2. Catalyst Composition and Coding**

| code | active metal loading (wt %) | support (wt %) |
|---|---|---|
| Picula cat B | Ni (58) and Pd (0.7) | $SiO_2$ (25) |
| Picula cat C | Ni (29) and Cu (3.7) | $SiO_2$ (8.8) and kaolin (50) |
| Picula cat D | Ni (58) and Cu (7) | $SiO_2$ (17.5) |
| Picula cat E | Ni (37) and Cu (2.3) | $SiO_2$ (12.6), $ZrO_2$ (37), and $La_2O_3$ (0.9) |

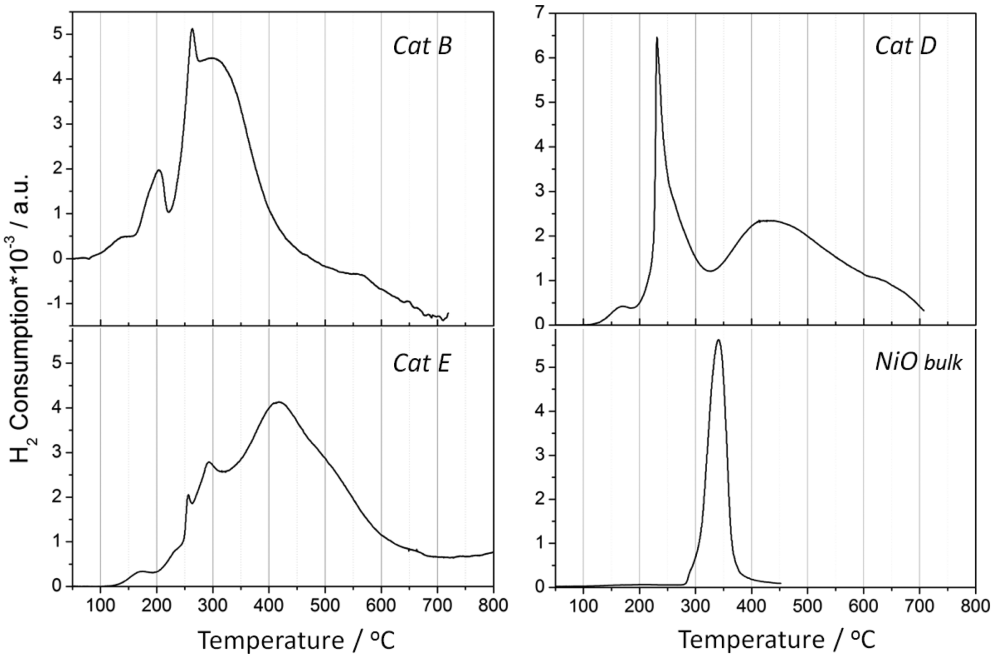


**Figure 1.** TPR profiles of cat B−E and bulk, unsupported NiO (TPR profile for cat C is similar to cat D).

$$\text{TG residue} = \frac{\text{mass of residue after heating to 900 °C}}{\text{mass sample (initial)}} \times 100\% \quad (3)$$

## 3. RESULTS AND DISCUSSION

**3.1. Catalyst Composition and Characterization.** Four bimetallic Picula catalysts were tested, three with Ni and Cu as the active metals and one with Ni in combination with Pd (Table 2). The support consists of silica, either as such or in combination with kaolin or $ZrO_2/La_2O_3$. The composition of the catalysts was analyzed with inductively coupled plasma (ICP), and the data are provided in Table 2. The sum of the active metals is higher than 30 wt % in all cases and up to 65 wt % for Picula cat D.

**3.2. TPR Studies on Fresh Catalysts.** Before actual catalytic experiments, the reduction temperature for the catalysts was determined using TPR, and the results are shown in Figure 1. The TPR profiles of catalysts B−E reveal a small, low-temperature reduction peak at 170 °C. This peak can be assigned to the reduction of traces of the higher $Ni^{III}$ oxide formed by oxygen chemisorption on well-dispersed NiO.[35] In addition, the TPR profiles of the NiCu catalysts (cat C/D and E in Figure 1) exhibit clear reduction peaks between 230 and 300 °C. The reduction of these catalysts starts at a lower temperature compared to bulk NiO (NiO bulk in Figure 1). This is accounted for by the better reducibility of $Ni^{II}$ to $Ni^0$ species in the presence of copper.

This effect can have various origins. On the one hand, it is suggested that, initially, copper reduction occurs and, thereafter, Cu produces spillover hydrogen, which considerably accelerates the nucleation of the Ni metal and enhances the reducibility of $Ni^{2+}$.[36] In our view, the most probable reason for NiO reduction at a low temperature compared to bulk NiO is close contact between NiO and CuO species as a consequence of the formation of a NiO−CuO solid solution. It is well-known that the molar free energy of reduction for copper oxide (−102 kJ/mol at 25 °C) is lower than for the corresponding nickel oxide (−12 kJ/mol at 25 °C).[37] Thus, it is likely that the Gibbs energy for reduction of the solid solution has a value between both of the extremes and that the Ni species are reduced at a lower temperature than in bulk NiO. Additional support for this hypothesis is the observation that the reduction of nickel and copper mixed oxides results in the formation of $Ni_xCu_y$ solid solutions.[23] The formation of $Ni_xCu_y$ solid solution in the case of cat C−E is also confirmed by XRD analysis (*vide infra*). Another possible explanation is that the reduced Cu particles on the NiO surface act as centers of nucleation, which induce reduction and growth of metallic Ni particles.[38]

A broad reduction peak is observed between 300 and 700 °C for cat C/D and E. In comparison, unsupported well-crystallized bulk NiO shows a single reduction peak with a maximum at 350 °C. This broad peak for cat C/D and E stems from $Ni^{II}$ species, which are by far more difficult to reduce than those related to the sharp reduction peaks below 300 °C and could be due to the presence of either surface nickel silicates or very small NiO particles. For cat D, it is also likely that peaks arising from the reduction of $Cu^{II}$ to $Cu^0$ are present in the temperature range of 200−230 °C. For instance, for Cu on silica, TPR spectra show CuO reduction peaks at around 220−250 °C.[39]

Cat C and D show similar TPR profiles, which is expected because cat C is prepared from cat D by mechanically mixing cat


DOI: 10.1021/acs.energyfuels.5b02223
Energy Fuels 2016, 30, 1544−1554

D with kaolin. The reduction of cat B, the only catalyst with Pd as the co-catalyst instead of Cu, also starts at lower temperatures than that of unsupported bulk NiO.

**3.3. Catalyst-Screening Studies with Fast Pyrolysis Oil in a Batch Setup.** Catalyst-screening studies on the hydrotreatment of pyrolysis oil with cat B−E were performed in a batch autoclave at an initial temperature of 150 °C (1 h), followed by 350 °C for 3 h. The initial pressure at 350 °C was about 200 bar. This two-stage heating profile was performed to reduce the tendency for coke formation.[13,40−42] For each experiment, a catalyst sieve fraction of 75−200 $\mu$m was used. The results were compared to data obtained for Ru/C, an extensively studied catalyst for fast pyrolysis oil upgrading.[12,21,40]

Relevant hydrogen uptakes and mass balance data are given in Table 3. The reactions for the Picula catalysts result in the formation of two immiscible liquid phases, a red−brown organic phase (total 37.4−44.3 wt % on feed) and a transparent, yellowish aqueous phase (32.9−42.5 wt % on feed), and gas-phase components other than hydrogen (7.4−9.4 wt % on feed). The organic liquid phase has a density higher than the water phase (see Figure 2 for a product from cat D). The reaction product obtained for Ru/C shows a black solid phase at the bottom, an intermediate, transparent water phase, and a dark brown top organic product phase (right panel of Figure 2). Hydrogen uptakes were between 160 and 270 NL/$kg_{PO}$. Duplicate experiments were performed with cat D and E, and the difference in the hydrogen uptake was less than 10%.

**Table 3. Hydrogen Consumption and Mass Balances for Catalytic Hydrotreatment of Fast Pyrolysis Oil Using Picula Cat B−E[a]**

| catalyst | cat B | cat C | cat D | cat E | Ru/C[b] |
|---|---|---|---|---|---|
| hydrogen uptake (NL/$kg_{PO}$) | 210 | 160 | 200 | 270 | 270 |
| yield (wet basis) | | | | | |
| oil product (wt % of feed) | 39.9 | 39.6 | 44.3 | 37.4 | 32.9 |
| aqueous phase (wt % of feed) | 32.9 | 39.1 | 35.3 | 42.5 | 43.7 |
| char (acetone insoluble) (wt % of feed)[c] | | | | | 1.13 |
| coke deposited on the catalyst (wt % on catalyst)[d] | 2.3 | 3.1 | 1.2 | 2.0 | nd[e] |
| gas (wt % of feed) | 8.0 | 8.8 | 7.4 | 9.4 | 15.6 |
| mass balance closure (wt %) | 81 | 88 | 87 | 89 | 93 |
| oxygen content of the oil product (wt %, dry) | 16.6 | 15.0 | 16.8 | 12.9 | 12.0 |
| moisture content of the oil product (wt %) | 4.69 | 4.56 | 3.99 | 6.53 | 1.98 |
| carbon content in the aqueous phase (wt %) | 7.9 | 8.9 | 9.3 | 6.5 | 5.2 |

[a]Hydrotreatment at 150 °C (1 h) and continued at 350 °C (3 h), with an initial pressure of 120 bar $H_2$ at room temperature. [b]Data for Ru/C taken from ref 34. [c]See the Materials and Methods for determination. [d]Determined by TGA (*vide infra*). [e]nd = not determined.

*3.3.1. Char Formation.* For Ru/C (Table 3) and NiCu-based catalysts with lower Ni metal loadings as in this study prepared by wet impregnation (instead of a sol−gel method),[23,24] an acetone-insoluble char is formed that is separated from the reaction mixture by solvent addition/centrifugation.[36] This char was not observed for the Picula catalysts (Table 3). In addition, only minor amounts of char/coke are observed on the catalysts (<3.3 wt %; Table 3). Apparently, the rate of char formation is less when using the Picula catalysts, although a comparison on coke formation for both catalysts could not be made.

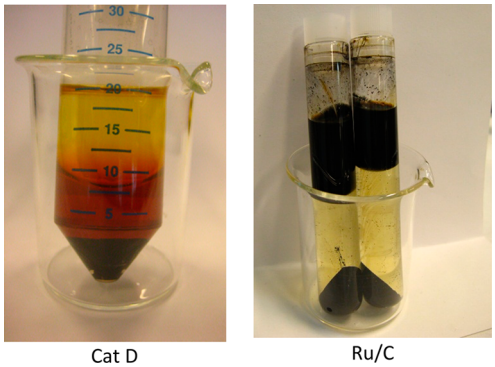


**Figure 2.** Liquid phases produced from the batch experiment with cat D (left) and Ru/C (right). Conditions: 150 °C (1 h) and 350 °C (3 h), with an initial pressure of 200 bar at 350 °C.

*3.3.2. Gas-Phase Components.* Typical gaseous components formed in the catalytic hydrotreatment reactions are $CO_2$, CO, $CH_4$, and small hydrocarbons ($C_2$−$C_3$). $CO_2$ and CO are likely produced by thermal/catalytic decarboxylation/decarbonylation reactions of aldehyde/ketones and/or carboxylic acids in the pyrolysis oil.[43] $CH_4$ is likely formed by either secondary methanation reactions of $CO_2$ and CO,[44,45] as a primary product from demethoxylation reactions of lignin fragments, or a combination thereof.

The amount of gas-phase components formed during the catalytic hydrotreatment reactions is provided in Figure 3. For Picula cat B−D, the amounts are a factor of 2 lower than for Ru/C and, particularly, methane is reduced considerably. This is a very positive feature of the Picula cat B−D, because lower methane production levels reduce carbon losses and lower hydrogen consumption. The only exception is cat E, showing a methane yield close to that for Ru/C. The high methane formation rate for this catalyst may be due to either a low amount of Cu in the catalyst formulation and/or the presence of $ZrO_2$. Ni is known to be capable of promoting the methanation of $CO_2$ and CO, whereas the addition of Cu reduces this tendency.[46,47] For cat E, the amount of Cu is the lowest of the catalyst formulations, and this may lead to higher methanation rates.

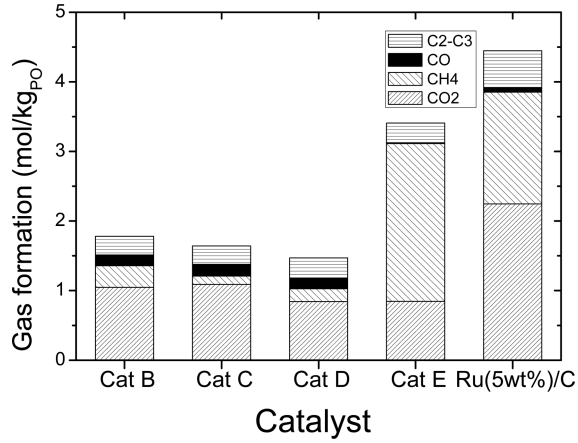


**Figure 3.** Gas formation for the batch hydrotreatment of fast pyrolysis oil with cat B−E. Conditions: 150 °C (1 h) and 350 °C (3 h), with an initial pressure of 200 bar at 350 °C.


DOI: 10.1021/acs.energyfuels.5b02223
*Energy Fuels* 2016, 30, 1544−1554

Also, the presence of $ZrO_2$ may play a role. $ZrO_2$ is reported to be less inert than $SiO_2$ for the hydrotreatment of pyrolysis oil (model) components.[48] For instance, it promotes hydrogenolysis of methoxy groups in guaiacol and, as such, favors the formation of methane and catechol.

*3.3.3. Catalyst Activity.* The activity of the various catalysts is defined on the basis of the $H_2$ uptake (section 2.5), and the results are depicted in Figure 4. Cat E shows the highest

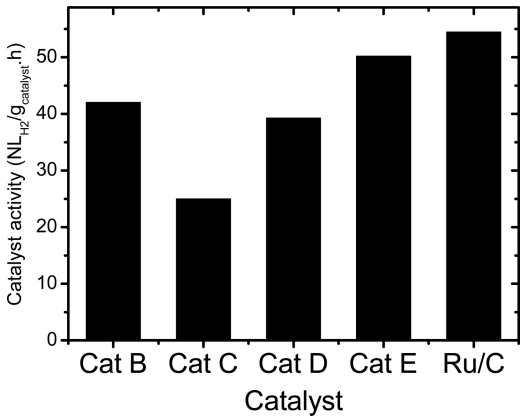


**Figure 4.** Catalyst activity for the Picula catalysts for the hydrotreatment of fast pyrolysis oil [150 °C (1 h) and 350 °C (3 h), with total initial pressure of 200 bar at 350 °C; activity based on total catalyst intake].

hydrogen uptake among the Picula catalysts tested, and cat C shows the least. The high hydrogen uptake of cat E is an overestimation of the activity because this catalyst yields the highest amount of gas phase (9.4 wt % on feed) and the lowest amount of product oil (32.9 wt % on feed; see Table 3). The gas phase contains the highest amounts of $CH_4$ (2.27 mol/$kg_{PO}$; see Figure 4), and this is the reason for the high hydrogen uptake. Methanation is not desired because it consumes large amounts of hydrogen without having a positive effect on the properties of the liquid organic phase.

When cat E is excluded for this reason, cat B has the highest activity per gram of catalyst, followed by cat D. Both cat B and D contain similar amounts of Ni (58 wt %). The main difference is the presence of Pd instead of Cu for cat B. In previous work,[25] we have shown that supported Cu catalysts do not display high hydro(-deoxy)genation activity, while Pd on a support is an active catalyst,[49] and this likely explains the difference in catalytic activity.

*3.3.4. Elemental Composition, Physical Properties, and the Molecular Composition of the Oil Products.* The elemental composition of the oil products obtained with Picula cat B–E is shown in a van Krevelen plot given in Figure 5 and compared to the result for an experiment in the absence of a catalyst. The atomic O/C ratios of the oil products are within a narrow range (0.12–0.17), while the H/C ratios show a much wider spread (1.32–1.51). Apparently, it is not possible to achieve full oxygen removal under the prevailing conditions. In addition, the non-catalytic run yields an organic product with an O/C ratio in the range for catalyzed reactions but with far lower H/C ratio. This particular product is a highly viscous paste, which is difficult to handle.

These results show that the O/C ratio only is not a good indicator for good product performance. Earlier studies on oil products obtained by Ni-based catalysts with low metal loadings prepared by wet impregnation confirm this and have shown that,

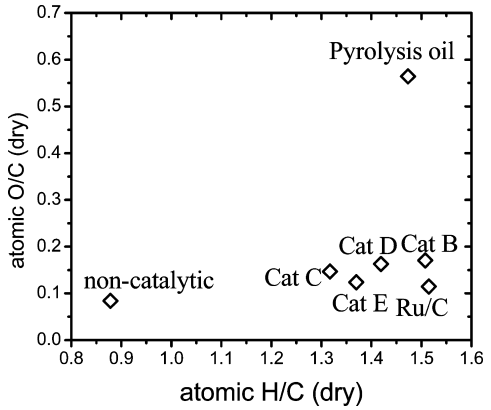


**Figure 5.** van Krevelen plot for the oil products [hydrotreatment at 150 °C (1 h) and 350 °C (3 h), with an initial pressure of 200 bar at 350 °C].

particularly, the H/C ratio is of prime importance.[23] In this respect, cat B and D are preferred because they give oil products with the highest H/C ratio.

Figure 6 shows the H/C ratio of the oil product versus the $H_2$ consumption during the hydrotreatment reaction. As expected,

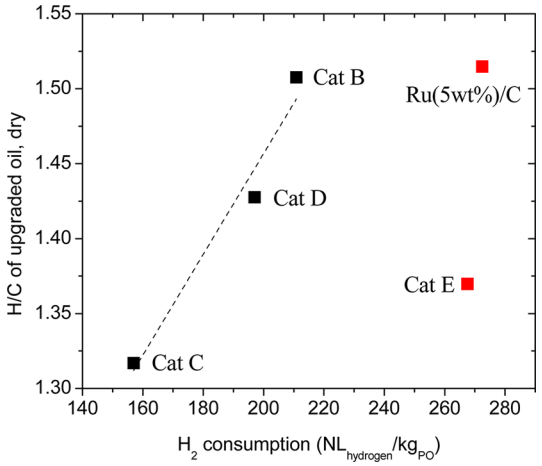


**Figure 6.** H/C ratio of the oil products versus $H_2$ consumption during the hydrotreatment of fast pyrolysis oil [150 °C (1 h) and 350 °C (3 h), with a total initial pressure of 200 bar at 350 °C].

for catalysts with a low methane production (cat B–D), the H/C ratio of the oil products correlates with the $H_2$ consumption. Cat E and Ru/C both yield significant amounts of methane (Figure 3), leading to higher hydrogen consumptions, explaining the deviations from the trend observed for the Picula cat B–D.

The residue after heating an oil product to 900 °C in $N_2$ in a TGA device (TG residue) appears as a good measure for the thermal stability of the sample,[50] and it also nicely correlates with the Conradson carbon residue (CCR) or micro carbon residue tester (MCRT) as used routinely in the petrochemical industry.[51] The TG residue of the organic products is given in Figure 7. The values are between 0.7 and 6.0 wt %, which is a considerable improvement compared to the fast pyrolysis oil feed (11.6 wt %). Best results were obtained for cat B (0.8 wt %), with a value close to that for Ru/C (0.7 wt %). The TG residue also correlates nicely with the H/C ratio, with lower TG residues for oil products with a higher H/C ratio (see Figure 7). Such relations are also found for fossil fuels.[52] A possible explanation is that the hydrogenation of the reactive groups (aldehydes/


DOI: 10.1021/acs.energyfuels.5b02223
*Energy Fuels* 2016, 30, 1544–1554

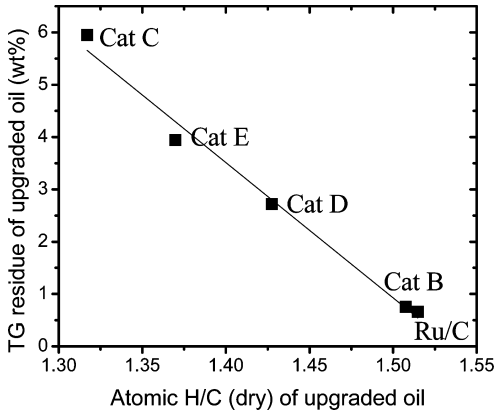


**Figure 7.** TG residue versus the H/C ratio of the oil products obtained from hydrotreatment at 150 °C (1 h) and 350 °C (3 h), with a total initial pressure of 200 bar at 350 °C.

ketones and sugars) in the fast pyrolysis oil feeds leads to the formation of less reactive molecules (alcohols, aromatics, and alkanes). The latter are less prone to coke formation at elevated temperatures.[53] High H/C ratios also indicate that the lignin fractions are converted into low-molecular-weight, monocyclic compounds instead of large, condensed molecules, such as polymeric aromatic hydrocarbons (PAHs, with a low H/C ratio), which are known coke precursors.[54]

For co-feeding applications, it is desirable that the oil products have a high solubility in hydrocarbons. As such, the solubility of the oil products in a model hydrocarbon mixture (hexane−benzene) was determined (see Table 4 for details). It is obvious that the oil products are more soluble in the model hydrocarbon mixture than the fast pyrolysis oil feed. However, none of the oil products obtained with cat B−E has a solubility close to the oil product from Ru/C. Apparently, the polarity of the oil products from cat B−E is higher than that for Ru/C.

The higher polarity of the oil products was also confirmed by $^1$H NMR measurements. The percentages of protons in various classes of organic products in the oils were classified using a procedure reported by Mullen et al.[55] (see Table 5 for details). The main difference between the oil products from the hydrotreatment with Picula cat B−E and Ru/C is the presence of lower amounts of alkanes in the products obtained with Picula cat B−E. These observations are in line with the solubility tests performed with the oil products, showing that the solubility of oil products using cat B−E in apolar hydrocarbon mixtures is lower than that for Ru/C. Apparently, alkane formation is reduced for cat B−D, indicating that hydrogenation of, for instance, aromatics and hydrodeoxygenation of small aldehydes and ketones occur to a lesser extent with these catalysts than with Ru/C.

The composition of the oil products was also analyzed with GC−MS/FID, and the results are given in Table 6. Several general trends are visible when comparing the composition of the oil products and the fast pyrolysis oil feed. The small sugars (such as levoglucosan) and non-aromatic aldehydes (such as hydroxyacetaldehyde) are absent after hydrotreatment, which demonstrates the high reactivity of these compounds. The acid content tends to increase slightly after hydrotreatment, particularly when considering that the water phase produced during the hydrotreatment reaction also contains significant amounts of organic acids (Table 7, *vide infra*). This suggests that the organic acids are rather inert under these conditions. Additional amounts of organic acids may be formed by reactions involving the sugar fraction of fast pyrolysis oil that are known to be able to form organic acids by acid-catalyzed reactions.[56] The amounts of non-aromatic ketones (such as cyclohexanone) slightly increase, which may be due to hydrogenation/hydrodeoxygenation of phenolics arising from the lignin fraction in fast pyrolysis oil. The content of non-aromatic ketones in the upgraded oil from Ru/C is low, indicating further hydrogenation of ketones into alcohols and alkanes. Oil products obtained with Picula cat B−E contain less alkanes than for Ru/C, in line with the $^1$H NMR data. Important to note here is that only a limited fraction of all compounds could be identified (19−33 wt %), because organic compounds with larger molecular weights in both the pyrolysis oil feed and the upgraded oils cannot be detected by GC−MS/FID.

*3.3.5. Aqueous Phase.* The aqueous phases after the hydrotreatment reaction with the Picula catalysts contain up to 9 wt % carbon (Table 3), indicative of the presence of polar organic molecules. Analysis with GC−MS/FID shows that the main components are low-molecular-weight organic acids and alcohols. The water phase does not contain substantial amounts of higher molecular weight, non-GC-detectable components, as was shown by GPC measurements.

*3.3.6. Concluding Remarks for the Catalyst-Screening Experiments.* On the basis of the screening experiments, cat B is the most promising catalyst because it produces an oil product with the highest H/C ratio (Figure 5), lowest TG residue (Figure 7), and highest solubility in a hydrocarbon model mixture. The good performance may be due to the presence of the noble metal Pd, which is replaced by Cu for the other Picula catalysts. On the basis of the product properties of the oil products, we conclude that polymerization is not occurring to a considerable extent in the early stage of the hydrotreatment reaction (Scheme 1). As a result, oil products with a lower molecular weight and a concomitant lower TGA residue are obtained. However, because Pd is by far more expensive per kilogram than Cu[57] (about 300 times), the latter is preferred. Of the Cu-promoted catalysts, cat D gave the best performance in terms of methane formation (low) and oil product properties (high H/C ratio and low TG residue).

**3.4. Catalyst Regenerability.** To anticipate the possible deactivation at very long times on stream, some of the catalysts tested were regenerated by calcination in air and the catalysts were characterized afterward. It is desirable to perform the calcination at a temperature as low as possible to prevent the destruction of the catalyst; however, it is also important that possible carbon deposits are (nearly) quantitatively removed. To determine the optimum calcination temperature for the spent catalysts, two different calcination approaches were applied, both using TGA. The first approach (isothermal mode) involves heating the catalysts to the preset temperature (300 °C) and maintaining the sample at this temperature for 1 h. The second

**Table 4. Solubility of Pyrolysis Oil and Upgraded Oils in a Mixture of Hexane and Benzene**

| | pyrolysis oil | cat B | cat C | cat D | cat E | Ru/C |
|---|---|---|---|---|---|---|
| solubility in the hexane−benzene (HB) mixture ($g_{oil}/g_{HB}$) | 0.01 | 0.21 | 0.11 | 0.16 | 0.18 | >0.49 |



DOI: 10.1021/acs.energyfuels.5b02223
*Energy Fuels* 2016, 30, 1544−1554

Table 5. $^1$H NMR Data for the Oil Products Obtained with Picula Cat B–E[a]

| shift (ppm) | proton assignment | pyrolysis oil | catalyst | | | | |
|---|---|---|---|---|---|---|---|
| | | | cat B | cat C | cat D | cat E | Ru/C |
| 10.1–9.5 | aldehydes | 0.8 | | | | | |
| 8.5–6.0 | (hetero)-aromatics | 14.9 | 11.4 | 8.4 | 5.0 | 5.4 | 7.6 |
| 6.0–4.4 | methoxy, carbohydrates | 15.6 | | | | | |
| 4.4–3.0 | alcohols, methylene–dibenzene | 18.8 | 7.1 | 2.3 | 5.0 | 2.8 | 3.3 |
| 3.0–1.5 | aliphatics $\alpha$ to heteroatom or unsaturation | 28.6 | 39.9 | 36.4 | 25.7 | 20.6 | 36.2 |
| 1.2–0.5 | alkanes | 18.2 | 41.7 | 34.5 | 23.2 | 20.9 | 52.9 |
| | aliphatics/aromatics ratio | 3.1 | 7.2 | 8.4 | 9.7 | 7.6 | 11.7 |

[a]Numbers are in percentage of the total proton integration area. The upgraded oils were obtained by a catalytic hydrotreatment at 150 °C (1 h) and 350 °C (3 h), at a total initial pressure of 200 bar at 350 °C.

Table 6. Composition by GC–MS/FID of the Product Oils[a] (in Weight Percent, Wet)

| | pyrolysis oil | cat B | cat C | cat D | cat E | Ru/C |
|---|---|---|---|---|---|---|
| acids | 2.75 | 3.37 | 2.95 | 1.96 | 4.09 | 5.98 |
| non-aromatic alcohols | 0.24 | 4.53 | 0.98 | 2.82 | 1.96 | 0.34 |
| non-aromatic aldehydes | 7.44 | | | | | |
| non-aromatic ketones | 4.18 | 15.79 | 10.25 | 12.15 | 9.21 | 4.07 |
| furans | 2.67 | 3.88 | 1.34 | 3.39 | 3.39 | 2.02 |
| pyrans | 0.88 | 0.64 | 0.08 | 0.33 | 0.20 | 0.19 |
| sugars | 3.43 | | | | | |
| catechols | 0.05 | | | | | |
| aromatic aldehydes | 0.01 | | | | | |
| lignin-derived phenols | 0.07 | 1.11 | 1.21 | 1.03 | 1.48 | 2.69 |
| guaiacols (methoxy phenols) | 2.90 | 1.69 | 1.71 | 2.07 | 1.88 | 4.83 |
| alkanes | | 0.82 | 0.32 | 0.55 | 0.71 | 7.19 |
| miscellaneous | 0.65 | 1.08 | 0.65 | 2.37 | 0.62 | 0.86 |
| total | 25.27 | 32.91 | 19.48 | 26.66 | 23.55 | 28.15 |

[a]The oil products were obtained by a catalytic hydrotreatment at 150 °C (1 h), followed by 350 °C (3 h), at a total initial pressure of 200 bar at 350 °C.

Table 7. Main Components (in Weight Percent, Wet) in the Aqueous Products by GC–MS/FID Analyses[a]

| | catalyst | | | | |
|---|---|---|---|---|---|
| | cat B | cat C | cat D | cat E | Ru/C |
| methyl alcohol | 1.54 | 1.58 | 1.98 | 0.39 | 0 |
| isopropyl alkohol | 0.26 | 0.85 | 0.33 | 0.33 | 0 |
| acetic acid | 3.34 | 5.44 | 3.66 | 4.02 | 3.39 |
| propanoic acid | 0.60 | 0.98 | 0.61 | 1.00 | 0.68 |
| butyric acid | 0.24 | 0.27 | 0.24 | 0.29 | 0.37 |
| pentanoic acid | 0.06 | 0.06 | 0.06 | 0.08 | 0.02 |

[a]Hydrotreatment at 150 °C (1 h) and continued at 350 °C (3 h), with a total initial pressure of 200 bar at 350 °C.

Table 8. TGA Results Using Isothermal and Dynamic Modes of Calcination[a]

| catalyst[b] | isothermal mode (300 °C for 1 h) | | dynamic mode (25–600 °C) | |
|---|---|---|---|---|
| | weight loss[c] (wt %) | weight increase[d] (wt %) | weight loss (wt %) | weight increase (wt %) |
| cat B | 2.3 | 1.9 | 2.2 | 14.4 |
| cat C | 3.1 | 0.1 | 3.3 | 1.5 |
| cat D | 1.2 | 1.8 | 1.3 | 14.6 |
| cat E | 2.0 | 0.3 | 2.1 | 3.2 |

[a]Calcination performed in TGA under air. [b]Hydrotreatment performed at 150 °C (1 h) and 350 °C (3 h), with a total pressure of 200 bar at 350 °C. The catalyst sieve fraction is 75–200 $\mu$m. [c]Mass loss as a result of burning of coke deposited on the catalyst surface. [d]Increase in catalyst weight as a result of oxidation of metallic species after coke removal.

approach (dynamic mode) involves heating the catalysts with a constant heating rate of 10 °C/min from ambient temperature to 600 °C. The TGA results are given in Table 8.

Spent cat B–E were calcined at a constant temperature of 300 °C (1 h) as well as heating from 25 to 600 °C. The weight loss is most likely due to oxidation of the coke/char deposited on the catalyst. The amounts are relatively small and indicate limited repolymerization of reactive intermediates and deposition on the catalyst surface in the course of the hydrotreatment reaction. However, after coke/char oxidation, the weight of the samples increases, indicating that oxidation of the active metals in the catalysts occurs to a significant extent. This effect is particularly evident in the dynamic mode, where the temperature is increased to 600 °C. As such, the results indicate that a balance has to be found between coke removal by oxidation and undesirable oxidation of the metals in the samples. It was decided to regenerate at a medium temperature of 300 °C for 1 h to prevent excessive oxidation. Thereafter, the catalysts were heated to 400 °C for nearly complete burning of residual carbon species. The latter temperature was selected because the fresh catalysts were also calcined at this temperature.

After regeneration, the catalysts were treated in a reductive medium (0.1 MPa $H_2$, 350 °C, flow rate of 100 $cm^3$/min, and 1 h) and characterized.

The XRD patterns of fresh and reduced cat B–E and spent samples after regeneration/reduction are presented in Figure 8. The XRD patterns of fresh and reduced cat B and D (Figure 8) show broad peaks, which are assigned to a NiO phase, with a



DOI: 10.1021/acs.energyfuels.5b02223
Energy Fuels 2016, 30, 1544–1554

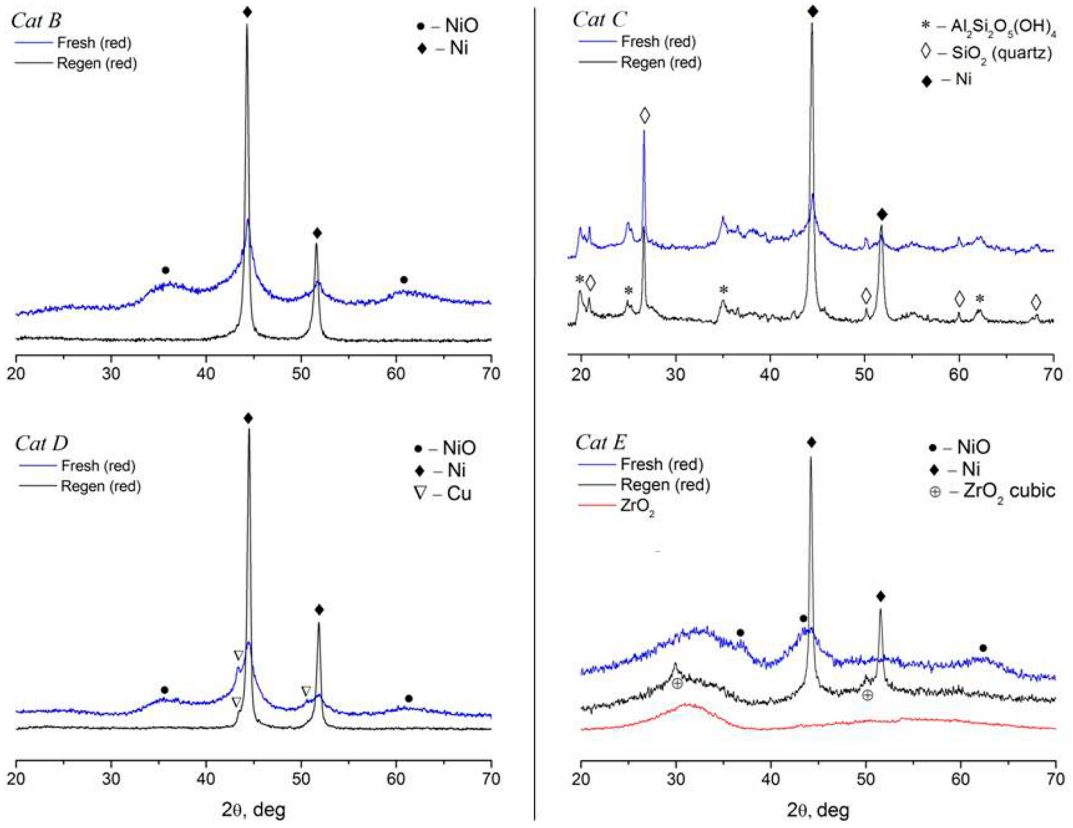


**Figure 8.** XRD patterns of cat B–E after reduction (0.1 MPa $H_2$, 350 °C, and 1 h) and passivation by ethanol and spent regenerated cat B–E after the same reduction procedure.

**Table 9. Textural Properties of the Fresh and Regenerated (+Reduced[a]) Catalysts**

| | fresh catalysts | | | | regenerated catalysts | | | |
|---|---|---|---|---|---|---|---|---|
| | $A_{BET}$ ($m^2/g$) | $V_{pores}$ ($cm^3/g$) | $V_{micropores}$ ($cm^3/g$) | average pore diameter (Å) | $A_{BET}$ ($m^2/g$) | $V_{pores}$ ($cm^3/g$) | $V_{micropores}$ ($cm^3/g$) | average pore diameter (Å) |
| catalyst[b] | | | | | | | | |
| cat B | 164 | 0.16 | | 39 | 15 | 0.07 | | 188 |
| cat C | 112 | 0.15 | | 55 | 25 | 0.13 | | 202 |
| cat D | 142 | 0.11 | 0.03 | 24 | 15 | 0.06 | | 153 |
| cat E | 66 | 0.05 | 0.002 | 30 | 32 | 0.06 | | 74 |

[a]Reduction at 350 °C (1 h), 0.1 MPa $H_2$, heating rate of 10 °C/min, and flow rate of 100 $cm^3$/min. [b]Hydrotreatment performed at 150 °C (1 h) and 350 °C (3 h), with a total pressure of 200 bar at 350 °C.

slight shift compared to the reference data. The broadness of the peaks indicates the presence of small-sized NiO crystallites. However, NiO species strongly interacting with $SiO_2$ by the formation of silicate-like structures may also contribute to these peaks. The absence of any reflections around 2$\theta$ of 22° and 26.6° indicates that $SiO_2$ is present in an amorphous phase[58] but could also be evidence for strong interactions between $SiO_2$ and NiO clusters in the samples.

The XRD patterns of fresh cat B and D after reduction show the presence of reflections at 2$\theta$ values of 44.4° and 51.7°, which correspond to a metallic Ni phase. The XRD patterns of spent cat B and D after regeneration and subsequent reduction reveal only the reflections of metallic nickel. The intensity of these reflections is increased in comparison to the fresh, reduced catalysts. In addition, the lines corresponding to the NiO phase are absent in the XRD patterns, indicating complete reduction of nickel in the case of regenerated catalysts. A slight shift of the metallic nickel peaks toward smaller 2$\theta$ angles is observed, pointing to the formation of a $Ni_xCu_y$ solid solution. The lines of metallic copper are also present in the XRD patterns of cat D.

The XRD patterns of fresh and regenerated cat C are similar and reveal lines corresponding to $SiO_2$ (quartz) and $Al_2Si_2O_5(OH)_4$ (kaolinite). This is expected because cat C is a physical mixture of cat D and kaolin. The main differences between the samples are the intensity and width of the metallic nickel peaks. The metallic nickel crystal size distribution (CSD) increases from 150 to 230 Å for the regenerated sample, indicative of some metal agglomeration. The same tendency is observed for the other catalysts (Table 10).

The diffraction pattern of fresh cat E after pre-reduction shows broadened peaks from a NiO phase, which indicates incomplete reduction of nickel. In the 2$\theta$ range of 25–40°, a halo is present, which is likely due to the $ZrO_2$ support. After catalyst regeneration, the halo remains and two lines attributed to a cubic modification of $ZrO_2$ emerge (2$\theta$ of 29.9° and 50°) likely as a result of structural rearrangements. The NiO peaks are absent


DOI: 10.1021/acs.energyfuels.5b02223
Energy Fuels 2016, 30, 1544–1554

in samples of regenerated cat E, indicative of complete reduction of the $Ni^{2+}$ species.

The textural and structural properties of the catalysts before reaction and spent catalysts after regeneration are given in Tables 9 and 10.

**Table 10. Ni CSD Size of the Fresh (after Reduction)[a] and Regenerated (+Reduced) Catalysts**

| | Ni CSD size (Å) | |
|---|---|---|
| | reduced | regenerated + reduced |
| catalyst[b] | | |
| cat B | 60 | 320 |
| cat C | 150 | 230 |
| cat D | 50 | 370 |
| cat E | 50 | 380 |

[a]Reduction at 350 °C (1 h), 0.1 MPa $H_2$, heating rate of 10 °C/min, and flow rate of 100 $cm^3$/min. [b]Hydrotreatment performed at 150 °C (1 h) and 350 °C (3 h), with a total pressure of 200 bar at 350 °C.

As seen from Table 9, the specific surface area and other textural properties of the catalysts change after reaction, regeneration, and reduction. The data suggest that considerable metal sintering occurs, in line with the XRD data (Table 10). Taking into account that the catalysts under study have high Ni loadings, it is proposed that the metallic species provide a greater part of the specific surface area of the reduced catalysts. Thus, the apparent decrease of the specific surface area in the case of regenerated catalysts is likely due to agglomeration of metallic particles.

This statement is supported by HRTEM measurements. HRTEM images of cat B [fresh, after reduction (images 1 and 2) and regenerated and reduced (images 3 and 4)] are shown in Figure 9. It is evident that the fresh reduced sample possesses a lamellar structure with thin flakes (1−2 nm), likely arising from oxide silicate species. Nickel is uniformly distributed throughout the catalyst. After the reaction and regeneration of the spent catalyst, agglomeration of Ni particles occurs. Similar changes are observed for all other catalysts (not shown for brevity).

Metal sintering seems an important phenomenon during the hydrotreatment reaction, as a result of either agglomeration during the reactions or the reductive pretreatment of the regenerated catalysts.

## 4. CONCLUSION

Ni-based Picula catalysts with a high Ni loading prepared by a sol−gel method are active catalysts for the hydrotreatment of fast pyrolysis oil. The catalysts show clear advantages compared to the benchmark Ru/C catalyst, viz., low methane production rates, limiting hydrogen usage, and low char formation rates. Detailed oil product analyses indicate that the reduced tendency for char formation is likely due to a high hydrogenation activity of the Picula catalysts in the low temperature range (below 200 °C). Here, the rate of hydrogenation should be high compared to the rate of polymerization reactions to avoid the formation of higher molecular weight fragments and eventually char. For Picula catalysts, this is certainly the case, whereas the hydrogenation activity of Ru/C is lower and in the range of the polymerization reactions. Further study on the long-term stability of cat D in continuous setups and testing of the oil products for co-processing in refinery units are in progress and will be published in due course. Regeneration studies on spent catalysts revealed that reactivation is possible, although some active metal agglomeration was observed. Research to identify promoters to reduce agglomeration is in progress.

## AUTHOR INFORMATION

### Corresponding Author

*E-mail: h.j.heeres@rug.nl.

### Notes

The authors declare no competing financial interest.

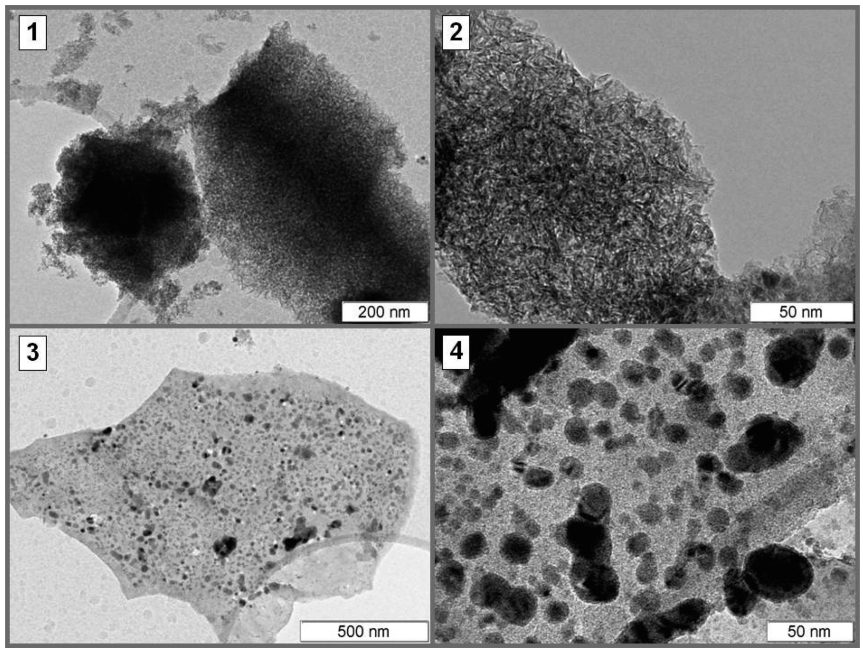


**Figure 9.** HRTEM images of cat B ($NiPd/SiO_2$): 1 and 2, fresh catalyst after reductive pretreatment (350 °C, 0.1 MPa $H_2$, heating rate of 10 °C/min, flow rate of 100 $cm^3$/min, and 1 h); 3 and 4, regenerated catalyst after reductive pretreatment at the same conditions.



DOI: 10.1021/acs.energyfuels.5b02223
*Energy Fuels* 2016, 30, 1544−1554

## ■ ACKNOWLEDGMENTS

The authors express their gratitude to Hans van der Velde and G. O. R. Alberda van Ekenstein (University of Groningen) for the EA, inductively coupled plasma−optical emission spectroscopy (ICP−OES), and TGA. Michael Windt and Dietrich Meier (von Thünen Institute, Hamburg, Germany) are acknowledged for recording and interpretation of the GC−MS/FID spectra. Finally, the BIOCOUP Project (EU Sixth Framework Project, Contract 518312) is acknowledged for financial support.

## ■ REFERENCES

(1) McKendry, P. *Bioresour. Technol.* **2002**, *83*, 37−46.
(2) Chiaramonti, D.; Oasmaa, A.; Solantausta, Y. *Renewable Sustainable Energy Rev.* **2007**, *11*, 1056−1086.
(3) Bridgwater, A.; Meier, D.; Radlein, D. *Org. Geochem.* **1999**, *30*, 1479−1493.
(4) de Wild, P.; den Uil, H.; Reith, J.; Kiel, J.; Heeres, H. *J. Anal. Appl. Pyrolysis* **2009**, *85*, 124−133.
(5) Kou, Y.; Wang, H.; Zhang, H.; Yang, X. *Catal. Today* **1999**, *51*, 47−57.
(6) Oasmaa, A.; Kuoppala, E. *Energy Fuels* **2003**, *17*, 1075−1084.
(7) Fogassy, G.; Thegarid, N.; Toussaint, G.; van Veen, A. C.; Schuurman, Y.; Mirodatos, C. *Appl. Catal., B* **2010**, *96*, 476−485.
(8) de Miguel Mercader, F.; Groeneveld, M.; Kersten, S.; Way, N.; Schaverien, C.; Hogendoorn, J. *Appl. Catal., B* **2010**, *96*, 57−66.
(9) Thegarid, N.; Fogassy, G.; Schuurman, Y.; Mirodatos, C.; Stefanidis, S.; Iliopoulou, E.; Kalogiannis, K.; Lappas, A. *Appl. Catal., B* **2014**, *145*, 161−166.
(10) Gueudré, L.; Thegarid, N.; Burel, L.; Jouguet, B.; Meunier, F.; Schuurman, Y.; Mirodatos, C. *Catal. Today* **2015**, *257*, 200−212.
(11) Vitolo, S.; Bresci, B.; Seggiani, M.; Gallo, M. *Fuel* **2001**, *80*, 17−26.
(12) de Miguel Mercader, F.; Groeneveld, M. J.; Kersten, S. R.; Geantet, C.; Toussaint, G.; Way, N. W.; Schaverien, C. J.; Hogendoorn, K. J. *Energy Environ. Sci.* **2011**, *4*, 985−997.
(13) Elliott, D. C.; Neuenschwander, G. G. In *Developments in Thermochemical Biomass Conversion*; Bridgwater, A. V., Boocock, D. G. B., Eds.; Blackie Academic & Professional: London, U.K., 1996; Vol. *1*, pp 611−621.
(14) Elliott, D. C. *Energy Fuels* **2007**, *21*, 1792−1815.
(15) Wildschut, J. Ph.D. Thesis, University of Groningen, Groningen, Netherlands, 2009; ISBN: 978-90-367-4113-2.
(16) Wildschut, J.; Melian-Cabrera, I.; Heeres, H. *Appl. Catal., B* **2010**, *99*, 298−306.
(17) Wildschut, J.; Iqbal, M.; Mahfud, F. H.; Cabrera, I. M.; Venderbosch, R. H.; Heeres, H. J. *Energy Environ. Sci.* **2010**, *3*, 962−970.
(18) Mercader, F.; Groeneveld, M.; Kersten, S.; Venderbosch, R.; Hogendoorn, J. *Fuel* **2010**, *89*, 2829−2837.
(19) Wang, H.; Male, J.; Wang, Y. *ACS Catal.* **2013**, *3*, 1047−1070.
(20) Ruddy, D. A.; Schaidle, J. A.; Ferrell, J. R., III; Wang, J.; Moens, L.; Hensley, J. E. *Green Chem.* **2014**, *16*, 454−490.
(21) Venderbosch, R. H.; Ardiyanti, A. R.; Wildschut, J.; Oasmaa, A.; Heeres, H. J. *J. Chem. Technol. Biotechnol.* **2010**, *85*, 674−686.
(22) Gutierrez, A.; Kaila, R.; Honkela, M.; Slioor, R.; Krause, A. *Catal. Today* **2009**, *147*, 239−246.
(23) Ardiyanti, A. R.; Khromova, S.; Venderbosch, R. H.; Yakovlev, V.; Heeres, H. J. *Appl. Catal., B* **2012**, *117−118*, 105−117.
(24) Ardiyanti, A. R.; Khromova, S.; Venderbosch, R. H.; Yakovlev, V.; Melián-Cabrera, I.; Heeres, H. J. *Appl. Catal., A* **2012**, *449*, 121−130.
(25) Ardiyanti, A. R.; Khromova, S. A.; Yakovlev, V. A.; Venderbosch, R. H.; Heeres, H. J. *Proceedings of the International Conference on Catalysis for Renewable Sources*; St. Petersburg, Russia, June 28−July 2, 2010.
(26) Yakovlev, V.; Khromova, S.; Sherstyuk, O.; Dundich, V.; Ermakov, D. Y.; Novopashina, V.; Lebedev, M. Y.; Bulavchenko, O.; Parmon, V. *Catal. Today* **2009**, *144*, 362−366.
(27) Ermakova, M. A.; Ermakov, D. Y. *Appl. Catal., A* **2003**, *245*, 277−288.
(28) Mercera, P.; Van Ommen, J.; Doesburg, E.; Burggraaf, A.; Roes, J. *Appl. Catal.* **1991**, *78*, 79−96.
(29) Zhao, C.; Kou, Y.; Lemonidou, A. A.; Li, X.; Lercher, J. A. *Chem. Commun.* **2010**, *46*, 412−414.
(30) Ali, A.; Zaki, M. *Thermochim. Acta* **2002**, *387*, 29−38.
(31) Yakovlev, V. A.; Khromova, S. A.; Ermakov, D. Y.; Parmon, V. N.; Venderbosch, R. H.; Heeres, H. J.; Ardiyanti, A. R. Russian Patent 2,440,847, 2012.
(32) Scherrer, P. *Nachr. Ges. Wiss. Goettingen, Math.-Phys. Kl.* **1918**, 98−100.
(33) Ardiyanti, A. R.; Gutierrez, A.; Honkela, M.; Krause, A.; Heeres, H. J. *Appl. Catal., A* **2011**, *407*, 56−66.
(34) Ardiyanti, A. R. Ph.D. Thesis, University of Groningen, Groningen, Netherlands, 2013; ISBN: 978-90-6182-234-5.
(35) Mile, B.; Stirling, D.; Zammitt, M. A.; Lovell, A.; Webb, M. *J. Catal.* **1988**, *114*, 217−229.
(36) Ashok, J.; Reddy, P. S.; Raju, G.; Subrahmanyam, M.; Venugopal, A. *Energy Fuels* **2009**, *23*, 5−13.
(37) Robertson, S.; McNicol, B.; De Baas, J.; Kloet, S.; Jenkins, J. *J. Catal.* **1975**, *37*, 424−431.
(38) Roman, A.; Delmon, B. *J. Catal.* **1973**, *30*, 333−342.
(39) Popa, T.; Zhang, Y.; Jin, E.; Fan, M. *Appl. Catal., A* **2015**, *505*, 52−61.
(40) Wildschut, J.; Mahfud, F. H.; Venderbosch, R. H.; Heeres, H. J. *Ind. Eng. Chem. Res.* **2009**, *48*, 10324−10334.
(41) Elliott, D. C.; Baker, E.; Piskorz, J.; Scott, D.; Solantausta, Y. *Energy Fuels* **1988**, *2*, 234−235.
(42) Elliott, D. C.; Oasmaa, A. *Energy Fuels* **1991**, *5*, 102−109.
(43) Şenol, O.; Viljava, T.; Krause, A. *Catal. Today* **2005**, *100*, 331−335.
(44) Jiménez, V.; Sánchez, P.; Panagiotopoulou, P.; Valverde, J. L.; Romero, A. *Appl. Catal., A* **2010**, *390*, 35−44.
(45) Panagiotopoulou, P.; Kondarides, D. I.; Verykios, X. E. *J. Phys. Chem. C* **2011**, *115*, 1220−1230.
(46) Araki, M.; Ponec, V. *J. Catal.* **1976**, *44*, 439−448.
(47) Sinfelt, J. H.; Carter, J.; Yates, D. *J. Catal.* **1972**, *24*, 283−296.
(48) Bui, V. N.; Laurenti, D.; Delichère, P.; Geantet, C. *Appl. Catal., B* **2011**, *101*, 246−255.
(49) Elliott, D. C.; Hu, J.; Hart, T. R.; Neuenschwander, G. G. Palladium catalyzed hydrogenation of bio-oils and organic compounds. U.S. Patent 7,425,657 B1, 2008.
(50) Ghetti, P. *Fuel* **1994**, *73*, 1918−1921.
(51) Noel, F. *Fuel* **1984**, *63*, 931−934.
(52) Trasobares, S.; Callejas, M. A.; Benito, A. M.; Martínez, M. T.; Severin, D.; Brouwer, L. *Ind. Eng. Chem. Res.* **1998**, *37*, 11−17.
(53) Oasmaa, A.; Kuoppala, E.; Ardiyanti, A.; Venderbosch, R. H.; Heeres, H. J. *Energy Fuels* **2010**, *24*, 5264−5272.
(54) Guisnet, M.; Magnoux, P. *Appl. Catal., A* **2001**, *212*, 83−96.
(55) Mullen, C. A.; Strahan, G. D.; Boateng, A. A. *Energy Fuels* **2009**, *23*, 2707−2718.
(56) Girisuta, B.; Danon, B.; Manurung, R.; Janssen, L.; Heeres, H. J. *Bioresour. Technol.* **2008**, *99*, 8367−8375.
(57) Kitco Metals, Inc. www.kitco.com (accessed Sept 2015).
(58) Guimon, C.; Auroux, A.; Romero, E.; Monzon, A. *Appl. Catal., A* **2003**, *251*, 199−214.


DOI: 10.1021/acs.energyfuels.5b02223
*Energy Fuels* 2016, 30, 1544−1554